STAR Results from the RHIC Beam Energy Scan-I

Lokesh Kumar (for the STAR Collaboration)[1]

Department of Physics, Kent State University, Kent, OH 44242

Abstract

The Beam Energy Scan (BES) program is being pursued at RHIC to study the QCD phase diagram, and search for the possible QCD phase boundary and possible QCD critical point. The data for Phase-I of the BES program have been collected for Au+Au collisions at center-of-mass energies ($\sqrt{s_{NN}}$) of 7.7, 11.5, 19.6, 27, and 39 GeV. These collision energies allowed the STAR experiment to cover a wide range of baryon chemical potential μ_B (100–400 MeV) in the QCD phase diagram. We report on several interesting results from the BES Phase-I covering the high net-baryon density region. These results shed light on particle production mechanism and freeze-out conditions, first-order phase transition and "turn-off" of QGP signatures, and existence of a critical point in the phase diagram. Finally, we give an outlook for the future BES Phase-II program and a possible fixed target program at STAR.

1. Introduction

The results from top RHIC energies suggest the existence of the Quark Gluon Plasma (QGP) [1]. The main task at hand now is to study the properties of the QGP and establish the QCD phase diagram. Lattice QCD calculations predict the transition between QGP and the hadronic gas as crossover at $\mu_B = 0$, while at large μ_B they predict a first order phase transition [2]. A point where the first order phase transition ends is called the critical point. Experimentally, the QCD phase diagram can be studied by colliding heavy ions at varying beam energies that can provide a T-μ_B region for each energy. Then, one can look at the various signatures for the phase boundary and critical point. We present results on (a) freeze-out parameters to get insight into the QCD phase diagram, (b) first and second coefficients (v_1, v_2) of the Fourier expansion of the angular distributions, dynamical charge correlations, and nuclear modification factor R_{CP} for the search of first-order phase transition and "turn-off" of QGP signatures, and (c) fluctuation measurements for the search of QCD critical point.

The first STAR proposal for the BES program [3] was made in the year 2008. This was followed by a successful data taking and physics analysis of a test run below injection energies at $\sqrt{s_{NN}}$ = 9.2 GeV [4]. The first phase of the BES program was started in the year 2010 with data taking at three low energies of 7.7, 11.5, and 39 GeV. In the year 2011, two more energy points were added at $\sqrt{s_{NN}}$ = 19.6 and 27 GeV.

---

[1] A list of members of the STAR Collaboration and acknowledgements can be found at the end of this issue.

The results presented here are based on the data collected by the STAR detector. STAR covers a large acceptance of 2π in azimuth (ϕ) and -1 to 1 in pseudorapidity (η). One of the important advantages which STAR possesses for the BES program is its almost uniform acceptance for different identified particles and collision energies at midrapidity. The main tracking device at STAR is the Time Projection Chamber (TPC), which provides momentum as well as particle identification (PID). For higher transverse momentum (p_T) region, the Time Of Flight (TOF) detector is quite effective in distinguishing different particles. Particles are identified using the ionization energy loss in TPC and time-of-flight information from TOF [5]. The centrality selection is done in STAR using the uncorrected charge particle multiplicity measured in the TPC within $|\eta| < 0.5$ [4].

2. Accessing QCD Phase Diagram

The QCD phase diagram is the variation of temperature T and baryon chemical potential μ_B. These quantities can be extracted from the measured hadron yields. Transverse momentum spectra for the BES Phase-I energies are obtained for π, K, p, Λ, Ξ, K_S^0, and ϕ [6]. The particle ratios are used to obtain the chemical freeze-out (a state when the yields of particles get fixed) conditions using the statistical thermal model (THERMUS) [7]. The two main extracted parameters are chemical freeze-out temperature T_{ch} and μ_B. Figure 1 (left panel) shows the variation of the extracted chemical freeze-out parameters using the Grand-Canonical Ensemble (GCE) approach of THERMUS for different energies and centralities [8]. We observe that at lower energies, T_{ch} shows a variation with μ_B as a function of centrality. Both T_{ch} and μ_B values seem to be decreasing from central to peripheral collisions. It may be noted that use of Strangeness Canonical Ensemble (SCE) shows an opposite trend, i.e. the T_{ch} values seem to increase from central to peripheral collisions [8]. However, it is found that the χ^2/NDF in case of SCE is higher for peripheral collisions [8]. More investigations are ongoing. In GCE the energy and quantum numbers or particle numbers are conserved on average through the temperature and chemical potentials. GCE is widely used in heavy-ion collisions. In the SCE, the strangeness (S) in the system is fixed exactly by its initial value of S, while the baryon and charge contents are treated grand-canonically. Although the T_{ch} shows an opposite trend between GCE and SCE, both results suggest the variation of chemical freeze-out parameters with centrality at lower energies.

The particle spectra can be used to obtain the kinetic freeze-out (a state when the spectral shapes of particles get fixed) conditions using the Blast Wave (BW) model [11]. The BW model is used to simultaneously fit the π, K, p spectra and the two relevant extracted parameters are kinetic freeze-out temperature T_{kin} and average flow velocity $\langle\beta\rangle$. Figure 1 (right panel) shows the variation of kinetic freeze-out parameters for different energies and centralities [8]. We observe that at a given collision energy, there is an anti-correlation between T_{kin} and $\langle\beta\rangle$. For a given collision centrality, the freeze-out temperature at high energy is lower and the average collectivity velocity $\langle\beta\rangle$ is larger due to expansion.

3. Search for First Order Phase Transition & Turn-off of QGP Signatures

3.1. Directed Flow

The directed flow v_1 is calculated as $\langle\cos(\phi - \Psi_1)\rangle$, where ϕ and Ψ_1 are the azimuthal angle of the produced particles and orientation of the first-order event plane, respectively. The directed
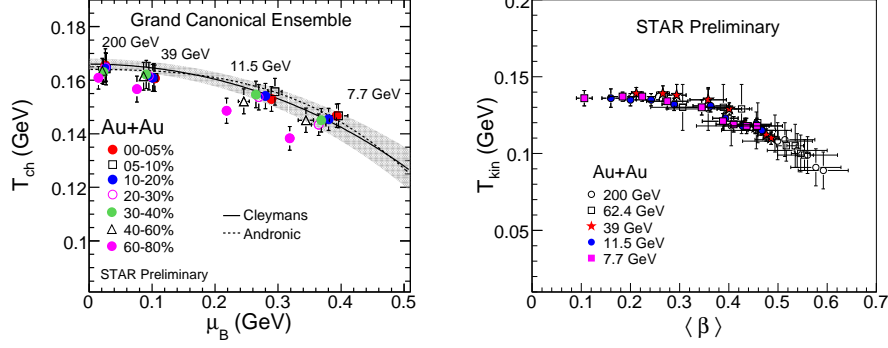
Figure 1: (Color online) Left panel: Variation of T_{ch} with μ_B for different energies and centralities. The curves represent the theoretical calculations [9, 10]. Right panel: Variation of T_{kin} with $\langle\beta\rangle$ for different energies and centralities. Errors in both panels represent the quadrature sum of systematic and statistical errors.

flow measurements near midrapidity for protons are considered as sensitive to the equation of state (EOS) and hence can be considered a phase transition signal [12]. Figure 2 shows the v_1
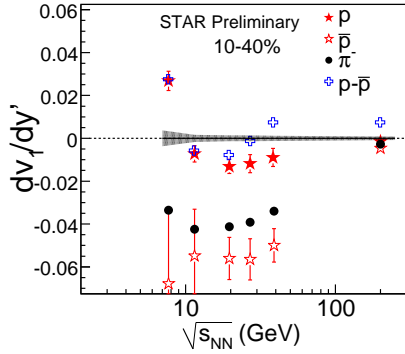

Figure 2: (Color online) Directed flow slope (dv_1/dy', $y'=y/y_{beam}$) for π^-, p, $\bar{p}$, and net-protons (p-$\bar{p}$) near midrapidity as a function of beam energy for mid-central (10–40%) Au+Au collisions. The shaded band refers to the systematic uncertainty on net-proton measurements.
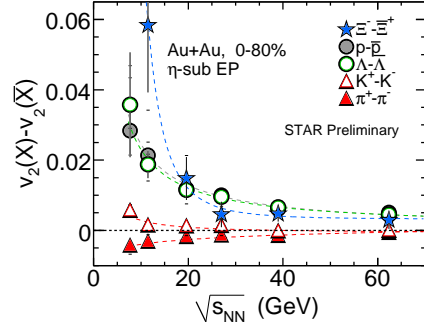
Figure 3: (Color online) The difference in v_2 between particles and their corresponding anti-particles as a function of beam energy in 0–80% Au+Au collisions. The curves represent fits to data points as discussed in text. Both statistical (vertical lines) and systematic errors (caps) are shown.

slope (dv_1/dy', where $y' = y/y_{beam}$ and y is rapidity), near midrapidity as a function of beam energy for the mid-central (10–40%) Au+Au collisions [13]. The pion and anti-proton v_1 slopes show negative values for all the beam energies studied. The proton v_1 slope changes sign while going from 7.7 GeV to 11.5 GeV and then stays negative up to 200 GeV. However, the net-protons v_1 slope (obtained using v_1 slopes of p, $\bar{p}$ and ratio of $\bar{p}/p$) changes sign two times going from lower to higher energy while showing a dip around $\sqrt{s_{NN}}$= 10–20 GeV. More studies are needed in order to understand these interesting observations.

3.2. Elliptic Flow

The elliptic flow v_2 is calculated as $\langle\cos 2(\phi - \Psi_2)\rangle$, where Ψ_2 is orientation of the second-order event plane. Elliptic flow mainly probes the early stages of heavy-ion collisions. At top RHIC energy of 200 GeV in Au+Au collisions, the elliptic flow scaled by the number of constituent quarks (n_q) vs. $(m_T - m_0)/n_q$ (where $m_T = \sqrt{p_T^2 + m_0^2}$) shows a scaling behavior where mesons and baryons have similar values at intermediate p_T. This is referred to as the number of constituent quark (NCQ) scaling [14]. It is an established signature of partonic matter formed in Au+Au collisions at 200 GeV and deviations from such scaling would indicate the dominance of hadronic interactions. Hence breaking of NCQ scaling at lower energies could be an indication of a "turn-off" of QGP signatures. Figure 3 shows the difference in v_2 of particles and
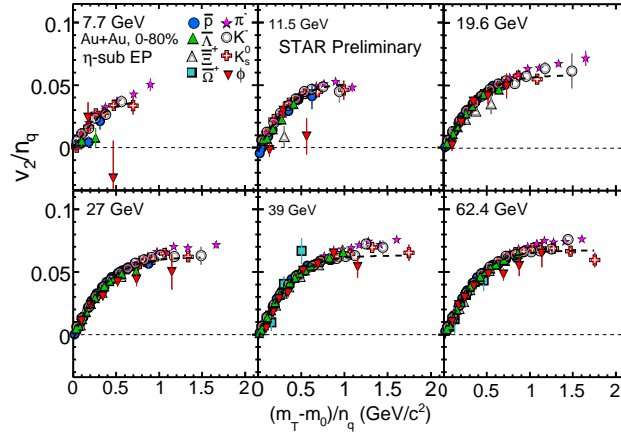

Figure 4: (Color online) v_2/n_q as a function of $(m_T - m_0)/n_q$ for different particles in Au+Au collisions at $\sqrt{s_{NN}}$ = 7.7, 11.5, 19.6, 27, 39 and 62.4 GeV. The errors shown are statistical only.

corresponding anti-particles as a function of beam energy [15]. The curves represent fits to data points with functional form: $f_{\Delta v_2}(\sqrt{s_{NN}}) = a\sqrt{s_{NN}}^{-b} + c$. The v_2 difference between particles and anti-particles is observed to increase when we go towards the lower energies. At low energies, $v_2(\pi^-) > v_2(\pi^+)$, $v_2(K^+) > v_2(K^-)$, and v_2(baryons) > v_2(anti-baryons). This difference between particles and anti-particles suggests that the NCQ scaling among particles and anti-particles is broken. However, the observed difference between v_2 of particles and anti-particles could be qualitatively explained by the models incorporating baryon transport at midrapidity and hadronic interactions [16]. We also observe that the baryons-mesons splitting for v_2 vs. $m_T - m_0$ starts to disappear for anti-particles at 11.5 GeV and below. Figure 4 shows the v_2/n_q vs. $(m_T - m_0)/n_q$ for different particles for $\sqrt{s_{NN}}$ = 7.7–62.4 GeV [15]. We observe that results for all the particles are consistent among each other within ±10% level, except for the ϕ-mesons. At the largest $m_T - m_0$ the ϕ-meson data points deviate by 1.8σ and 2.3σ for $\sqrt{s_{NN}}$ = 7.7 and 11.5 GeV, respectively. Since ϕ-mesons have smaller hadronic interaction cross-section, their smaller v_2 values could indicate that the hadronic interactions start to dominate over partonic effects for the systems formed at beam energies below $\sqrt{s_{NN}}$ = 11.5 GeV [17]. However, as can been seen from the figure, a higher statistics data are needed to extend the $m_T - m_0$ range and significance of the deviation observed.

4

3.3. Dynamical Charge Correlations

The dynamical charge correlations are studied through a three-particle mixed harmonics azimuthal correlator [18], $\gamma = \langle cos(\phi_\alpha + \phi_\beta - 2\Psi_{RP}) \rangle$. This observable represents the difference between azimuthal correlations projected onto the direction of the angular momentum vector and correlations projected onto the collision reaction plane. It is suggested that the difference in the
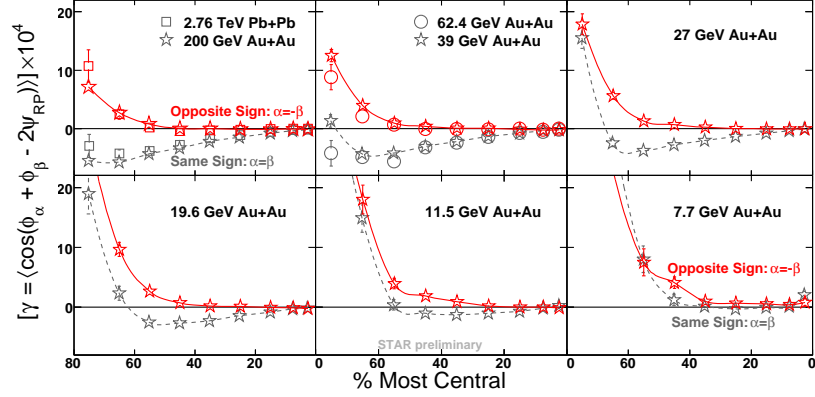

Figure 5: (Color online) $\langle cos(\phi_\alpha + \phi_\beta - 2\Psi_{RP}) \rangle$ as a function of centrality for Au+Au collisions at $\sqrt{s_{NN}}$ =7.7-200 GeV. For comparison, results for Pb+Pb collisions at 2.76 TeV are also shown. Errors are statistical only.

correlations between same sign and opposite sign charges in heavy-ion collisions could be related to local *parity* violation if there is a deconfinement and a chiral phase transition [19]. This is also referred to as Chiral Magnetic Effect (CME). At top RHIC energies, we observed a separation between the correlations of same and opposite sign charges. If this difference can be attributed to the QCD phase transitions, the absence of such observation could be an indication of the system which did not undergo the phase transition. Hence, the observable could be useful to locate the energy in the BES program where the QGP signature "turns off". Figure 5 shows the results for the beam energies from 7.7–200 GeV as a function of centrality [20]. For comparison, Pb-Pb results from ALICE are also shown [21] which are observed to be consistent with the results from top RHIC energy. The separation between same and opposite sign charges decreases with decreasing energy and vanishes below $\sqrt{s_{NN}}$ =11.5 GeV.

3.4. Nuclear Modification Factor

Another established signature of QGP at top RHIC energy is the Nuclear Modification Factor R_{CP}, which is defined as ratio of yields at central collisions to peripheral collisions, scaled by the corresponding number of binary collisions. It has been observed that at high p_T, the R_{CP} of different particles is less than unity [22], which is attributed to the energy loss of the partons in the dense medium. In the absence of dense medium, there may not be suppression of high p_T particles, which can serve as an indication of "turn-off" of a QGP signature. Figure 6 shows the R_{CP} of various strange hadrons such as K_S^0, ϕ, Λ, Ξ^-, and Ω^- in Au+Au collisions at $\sqrt{s_{NN}}$ =7.7– 39 GeV [23]. We observe that for $p_T > 2$ GeV/c, the $R_{CP}(K_S^0)$ is less than unity at 39 GeV and then the value increases as the beam energy decreases. For $\sqrt{s_{NN}} < 19.6$ GeV, $R_{CP}(K_S^0)$ is above unity, indicating decreasing partonic effects at lower energies. For (un)-identified charged hadrons results, please refer to [24].
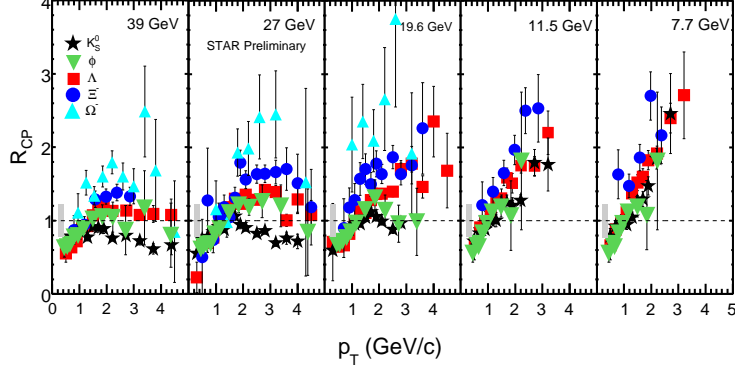
Figure 6: (Color online) R_{CP} (0–5% / 40%–60%) for K_S^0, Λ, Ξ^-, Ω^- and R_{CP} (0–10% / 40%–60%) for ϕ-meson in Au+Au collisions at $\sqrt{s_{NN}}$ =7.7–39 GeV. Errors are statistical only. Grey bands represent the normalization error from N_{bin}.

4. Search for QCD Critical Point

If a system passes close to a critical point, the correlation length ξ is expected to diverge. The higher moments (skewness S and kurtosis κ) of distributions of conserved quantities such as net-baryons, net-charge, and net-strangeness, have a better sensitivity to the correlation length compared to variance σ^2 [25]. Also, the moment products such as $\kappa\sigma^2$ and $S\sigma$ can be related to the ratios of order susceptibilities calculated in Lattice QCD and HRG model as $\kappa\sigma^2 = \chi_B^{(4)}/\chi_B^{(2)}$ and $S\sigma = \chi_B^{(3)}/\chi_B^{(2)}$ [26]. One of the advantages of using these products is that they cancel the volume effects. Figure 7 shows the $\kappa\sigma^2$ and $S\sigma$ for net-protons as a function of beam energy for different collision centralities [27]. For comparison, the results are shown for Poisson expectations and UrQMD model calculations [28]. The bottom panel shows the $S\sigma$ values normalized by the corresponding Poisson expectations. We observe that the moment products show similar values for central 0–5% and peripheral collisions for $\sqrt{s_{NN}}$ =39–200 GeV. For beam energies below 39 GeV, they have different values for central and peripheral collisions. Their values are below Poisson expectations for $\sqrt{s_{NN}}$ > 7.7 GeV for 0–5% central collisions. However, for peripheral collisions, moment products values are greater than Poisson expectations below 19.6 GeV. The UrQMD model calculations show a smooth monotonic behavior as a function of collision energy. It may be noted that we have large uncertainties for data points below 19.6 GeV that calls for higher statistics data for these energies. For net-charge and particle ratio fluctuation results, please refer to [29].

5. The BES Phase-II and STAR in Fixed Target Mode

The BES Phase-I program from STAR has several interesting results as discussed above. We have collected sizable data for Au+Au collisions over a wide range of collisions energies from 7.7 to 39 GeV. However, to consolidate the findings from Phase-I, we need higher statistics at lower energies, especially at 7.7 and 11.5 GeV. As we have discussed above, statistics for several important observables, such as ϕ-meson v_2 and higher moments of net-protons distributions, are not sufficient to draw quantitative conclusions. Also, there is more than a 100 MeV gap in μ_B between 11.5 and 19.6 GeV, so having one more energy point around 15 GeV would allow to confirm the trends happening between 11.5 and 19.6 GeV.
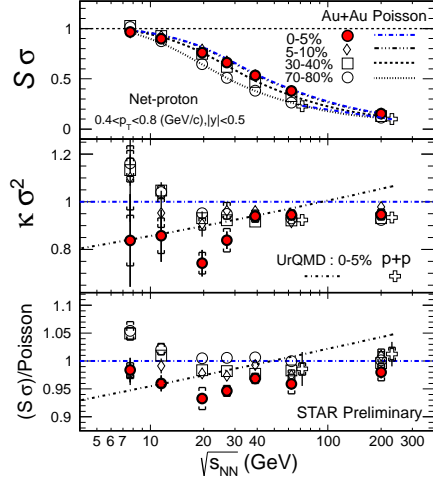
Figure 7: (Color online) $\kappa\sigma^2$, $S\sigma$ and $S\sigma$ values normalized by the Poisson expectation, as a function of collision energy. Vertical bars are statistical and caps are systematic errors.

Table 1: The collider mode $\sqrt{s_{NN}}$, fixed target mode $\sqrt{s_{NN}}$, and corresponding μ_B values. The μ_B values are listed for the central collisions corresponding to fixed target $\sqrt{s_{NN}}$ [10].

Collider mode $\sqrt{s_{NN}}$ (GeV)	Fixed-target mode $\sqrt{s_{NN}}$ (GeV)	μ_B (MeV)
19.6	4.5	585
15	4.0	625
11.5	3.5	670
7.7	3.0	720
5	2.5	775

In view of these, STAR has proposed a BES Phase-II program. For this STAR has requested an electron cooling device at RHIC to increase the luminosity for collisions below $\sqrt{s_{NN}} = 20$ GeV. Simulation results indicate that with electron cooling, the luminosity could be increased by a factor of about 3–5 at 7.7 GeV and about 10 around 20 GeV [30]. An additional improvement in luminosity may be possible by operating with longer bunches at the space-charge limit in the collider [31]. So overall improvement in luminosity could be about 10-fold. The luminosity improvement will not only allow the precision measurements of the above important observables but will also be helpful in the measurements of rare probes such as dilepton production and hypertriton measurements [32]. To maximize the use of collisions provided at STAR for the BES program, we have proposed to run STAR in "fixed-target mode". The main motivation for this proposal is to extend the μ_B coverage currently from 400 MeV to about 800 MeV so as to cover a large portion of the phase diagram. For this, we plan to install a fixed Au target in the beam pipe to perform the Au(beam)-Au(target) collisions. The data taking can be done concurrently during the normal RHIC running. This proposal will not affect the normal RHIC operations. Table 1 lists the proposed collision energies, corresponding fixed target center-of-mass energies, and baryon chemical potential values.

6. Summary

We have presented several interesting results from the STAR BES Phase-I program. Currently, STAR covers a large range of μ_B (20–400 MeV) in the phase diagram. We have observed a centrality dependence of freeze-out parameters at lower energies. We have looked at various observables for the search of first order phase transition, "turn-off" of the QGP signatures, and search of a QCD critical point. The observables such as v_1 slope, R_{CP} and v_2 of PID hadrons, and higher moments of net-proton distributions, show some dramatic changes for the energy range

7

$\sqrt{s_{NN}} < 20$ GeV. We have observed that proton v_1 slope changes sign between 7.7 and 11.5 GeV. The net-proton v_1 slope changes sign twice as a function of beam energy. We have observed a difference in v_2 of particles and corresponding anti-particles which increases with decreasing collision energy. The ϕ-meson v_2 deviates from that of other particles, the charge separation signal vanishes, and the R_{CP} of K_S^0 is greater than unity for beam energy of 11.5 GeV and below. The moment products have values below the Poisson expectation for 0–5% central Au+Au collisions. For peripheral collisions, they are above unity at $\sqrt{s_{NN}} < 19.6$ GeV. An electron cooling device at RHIC will significantly increase luminosity at beam energies below 20 GeV allowing the precision measurements for several important observables for phase structure studies. In addition, we propose to run STAR in fixed target mode which will extend the μ_B coverage from STAR up to 800 MeV in the phase diagram.

References

[1] J. Adams *et al.* (STAR Collaboration), Nucl. Phys. A **757**, 28 (2005).

[2] Y. Aoki *et al.*, Nature **443** 675, (2006).

[3] M. M. Aggarwal *et al.* (STAR Collaboration), arXiv:1007.2613; L. Kumar (for STAR Collaboration), Nucl. Phys. A **862**, 125 (2011); B. Mohanty, Nucl. Phys. A **830**, 899C (2009).

[4] B. I. Abelev *et al.* (STAR Collaboration), Phys. Rev. C **81**, 024911 (2010).

[5] M. Anderson *et al.*, NIM A **499**, 659 (2003); W. Llope (for STAR Collaboration), NIM A **661**, S110 (2012).

[6] L. Kumar (for STAR Collaboration), arXiv:1201.4203(2012), J. Phys. G: Nucl. Part. Phys. **38**, 124145 (2011); X. Zhu (for STAR Collaboration), Acta Phys. Polon. B Proc. Supp. **5**, 213 (2012).

[7] J. Adams *et al.* (STAR Collaboration), Nucl. Phys. A **757**, 102 (2005); J. Cleymans *et al.*, Comp. Phys. Comm. **180**, 84 (2009).

[8] S. Das (for STAR Collaboration), these proceedings.

[9] A. Andronic *et al.*, Nucl. Phys. A **834**, 237 (2010).

[10] J. Cleymans *et al.*, Phys. Rev. C **73**, 034905 (2006).

[11] E. Schnedermann *et al.*, Phys. Rev. C **48**, 2462 (1993).

[12] J. Brachmann *et al.*, Phys. Rev. C **61**, 024909 (2000); L. P. Csernai *et al.*, Phys. Lett. B **458**, 454 (1999); H. Stocker, Nucl. Phys. A **750**, 121 (2005).

[13] Y. Pandit (for STAR Collaboration), these proceedings.

[14] J. Adams *et al.* (STAR Collaboration), Phys. Rev. Lett. **95**, 122301 (2005).

[15] S. Shi (for STAR Collaboration), these proceedings.

[16] J. Dunlop *et al.*, Phys. Rev. C **84**, 044914 (2011); J. Xu *et al.*, Phys. Rev. C **85**, 041901 (2012).

[17] B. Mohanty and N. Xu, J. Phys. G **36**, 064022 (2009).

[18] B. I. Abelev *et al.* (STAR Collaboration), Phys. Rev. Lett. **103**, 251601 (2009).

[19] K. Fukushima *et al.*, Phys. Rev. D **78**, 074033 (2008).

[20] G. Wang (for STAR Collaboration), these proceedings.

[21] B. Abelev *et al.* (ALICE Collaboration), arXiv:1207.0900.

[22] M. A. C. Lamont (for the STAR Collaboration), J. Phys. Conf. Ser. **50**, 192 (2006).

[23] X. Zhang (for STAR Collaboration), these proceedings.

[24] E. Sangaline (for STAR Collaboration), these proceedings.

[25] M. A. Stephanov, Phys. Rev. Lett. **102**, 032301 (2009); M. A. Stephanov, Phys. Rev. Lett. **107**, 052301 (2011).

[26] S. Gupta *et al.*, Science **332**, 1525 (2011); F. Karsch and K. Redlich, Phys. Lett. B **695**, 136 (2011).

[27] X. Luo (for STAR Collaboration), these proceedings.

[28] M. Bleicher *et al.*, J. Phys. G: Nucl. Part. Phys. **25**, 1859 (1999).

[29] D. McDonald (for STAR Collaboration), these proceedings; P. Tribedy (for STAR Collaboration), these proceedings.

[30] A. Fedotov, and W. Fischer, Private communications, 2012.

[31] A. Fedotov and M. Blaskiewicz, BNL CAD Tech Note: C-A/AP/449 (February 10, 2012).

[32] B. Huang (for STAR Collaboration), these proceedings; Y. Zhu (for STAR Collaboration), these proceedings.